RESEARCH ARTICLE SUMMARY

NEURODEVELOPMENT

Structured spike series specify gene expression patterns for olfactory circuit formation

Ai Nakashima*, Naoki Ihara*, Mayo Shigeta, Hiroshi Kiyonari, Yuji Ikegaya, Haruki Takeuchi†

INTRODUCTION: The development of precise neural circuits is initially directed by genetic programming and subsequently refined by neural activity. In the mouse olfactory system, axons from various olfactory sensory neurons expressing the same olfactory receptor converge onto a few spatially invariant glomeruli, generating the olfactory glomerular map in the olfactory bulbs. During development, olfactory receptors instruct axon sorting to form discrete glomeruli. Olfactory receptors generate a combinatorial code of axon-sorting molecules whose expression is regulated by neural activity. However, it remains unclear how neural activity induces olfactory receptor–specific expression patterns of axon-sorting molecules.

RATIONALE: The prevailing model for the activity-dependent development of neural circuits postulates an interaction between pre- and postsynaptic neurons. In Hebbian plasticity, the correlated activity of pre- and postsynaptic neurons strengthens synaptic connections, whereas uncorrelated activity or lack of activity weakens them. However, this theory does not explain activity-dependent mechanisms in olfactory map formation. Axons of olfactory sensory neurons can converge to form glomerular-like structures even in mutant mice lacking synaptic partners, suggesting another activity-dependent mechanism for glomerular segregation. The involvement of neural activity in olfactory map formation has been demonstrated by experimental suppression of neural activity. Here, we asked how neural activity is involved in the expression of axon-sorting molecules regulating glomerular segregation.

ON OUR WEBSITE

Read the full article at http://dx.doi.org/10.1126/science.aaw5030

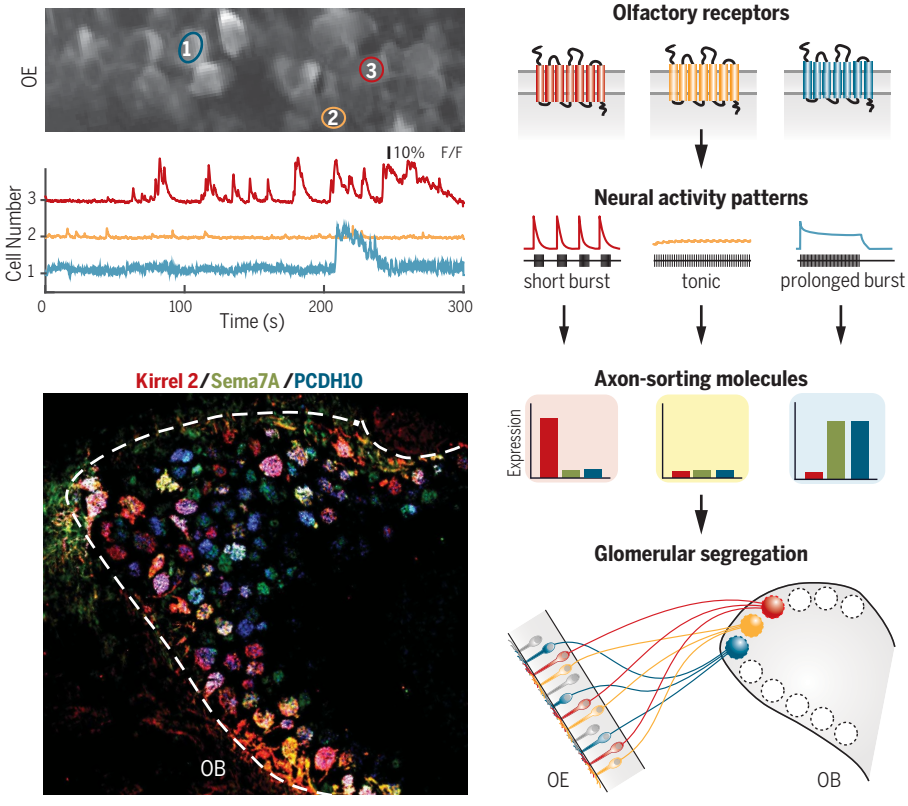

Firing pattern–dependent olfactory map formation. Top left: Diverse patterns of spontaneous neural activity in olfactory sensory neurons. Bottom left: A combinatorial expression pattern of axon-sorting molecules at axon termini of olfactory sensory neurons. Right: A model for activity-dependent olfactory map formation. OE, olfactory epithelium; OB, olfactory bulb. Axon-sorting molecules for glomerular segregation: red, Kirrel2 (kin of IRRE-like protein 2); green, Sema7A (semaphorin 7A); blue, PCDH10 (protocadherin 10).

RESULTS: We performed calcium imaging experiments and optogenetic stimulation to address how neural activity generates olfactory receptor–specific expression patterns of axon-sorting molecules. Calcium imaging of olfactory sensory neurons revealed that the temporal patterns of spontaneous neuronal spikes were not spatially organized, but rather were correlated with the olfactory receptor types. Receptor substitution experiments demonstrated that olfactory receptors determine spontaneous activity patterns. Moreover, optogenetically differentiated patterns of neuronal activity induced expression of corresponding axon-sorting molecules and regulated glomerular segregation.

CONCLUSION: We have demonstrated an instructive role of neural activity in olfactory map formation. We propose an activity-dependent mechanism, different from Hebbian plasticity theory, in which specific patterns of spontaneous activity determined by the expressed olfactory receptor type contribute to generating the combinatorial code of axon-sorting molecules for olfactory receptor–specific axon sorting.

Neural activity is involved in various aspects of brain development and function. Our findings show that in the olfactory system, gene expression that regulates neural circuit formation is dependent on neural firing patterns. With this strategy, neurons can generate variation through diversifying gene expression. The pattern-dependent gene regulation may also expand beyond development to plastic changes in neural circuits throughout the lifetime. ■

The list of author affiliations is available in the full article online.
*These authors contributed equally to this work.
†Corresponding author. Email: haruki-t@mol.f.u-tokyo.ac.jp
Cite this article as A. Nakashima *et al.*, *Science* **365**, eaaw5030 (2019). DOI: 10.1126/science.aaw5030

RESEARCH ARTICLE

NEURODEVELOPMENT

Structured spike series specify gene expression patterns for olfactory circuit formation

Ai Nakashima[1]*, Naoki Ihara[1]*, Mayo Shigeta[2], Hiroshi Kiyonari[2,3], Yuji Ikegaya[1,4], Haruki Takeuchi[1,5]†

Neural circuits emerge through the interplay of genetic programming and activity-dependent processes. During the development of the mouse olfactory map, axons segregate into distinct glomeruli in an olfactory receptor (OR)–dependent manner. ORs generate a combinatorial code of axon-sorting molecules whose expression is regulated by neural activity. However, it remains unclear how neural activity induces OR-specific expression patterns of axon-sorting molecules. We found that the temporal patterns of spontaneous neuronal spikes were not spatially organized but were correlated with the OR types. Receptor substitution experiments demonstrated that ORs determine spontaneous activity patterns. Moreover, optogenetically differentiated patterns of neuronal activity induced specific expression of the corresponding axon-sorting molecules and regulated axonal segregation. Thus, OR-dependent temporal patterns of spontaneous activity play instructive roles in generating the combinatorial code of axon-sorting molecules during olfactory map formation.

In the mammalian brain, the development of precise neural circuits is initially directed by intrinsic genetic programming and subsequently refined by neural activity (*1*–*3*). In the mouse olfactory system, individual olfactory sensory neurons (OSNs) express a single gene of a functional olfactory receptor (OR) out of >1000 OR genes (*4*–*6*). Axons from various OSNs expressing the same OR converge onto a few spatially invariant glomeruli, generating the olfactory glomerular map in the olfactory bulbs (OBs) (*7*–*9*). The olfactory glomerular map forms through two processes: global targeting and glomerular segregation (*10*, *11*). OSN axons are first guided to approximate target regions according to gradients of axon guidance molecules (*12*, *13*) and are subsequently sorted into specific glomerular structures in an activity-dependent manner (*11*, *14*–*16*). In glomerular segregation, OSN axons discriminate expressed OR types. Substitution of an OR-coding DNA sequence with another sequence results in allopatric generation of glomeruli that are distinct from the original ones (*17*, *18*). Further, suppression of spontaneous neural activity disrupts the glomerular segregation (*15*). However, it remains a mystery how neural activity mediates the OR-specific glomerular segregation.

The most prevailing model for the activity-dependent development of neural circuits postulates the interaction between pre- and postsynaptic neurons. In Hebbian plasticity (*19*), the correlated activity of pre- and postsynaptic neurons strengthens synaptic connections, whereas uncorrelated activity or lack of activity weakens them. However, this theory does not explain activity-dependent mechanisms for axon sorting before the formation of synapses. OSN axons are capable of converging to form glomerular-like structures even in mutant mice lacking synaptic partners (*20*, *21*). These findings suggest another activity-dependent mechanism for glomerular segregation.

OR molecules control the expression of various axon-sorting molecules, which serve to regulate glomerular segregation through their adhesive or repulsive interactions (*22*–*26*). These molecules exhibit both mosaic and glomerular-specific expression patterns (*27*). However, their spatial patterns are not identical in the OB. As a result, OR identity is represented as a unique combinatorial code of axon-sorting molecules at the axon termini, which provides the self-identification tags for OR-specific glomerular segregation. Because the expression of axon-sorting molecules is activity-dependent (*22*, *25*), neural activity is expected to bridge between the OR types and the combinatorial expression of the axon-sorting molecules. Previous studies reported that spontaneous firing rates are different among OSN classes in several species (*28*–*32*). However, it remains unclear whether neural activity functions in an instructive way or a permissive way; it is not clear whether specific features of neural activity patterns are important or whether the presence of neural activity is sufficient to trigger a predetermined gene expression. Here, we applied genetic approaches to address how neural activity generates OR-specific expression patterns of axon-sorting molecules.

Activity-dependent expression of axon-sorting molecules

On the basis of our previous study (*27*), we focused on Kirrel2, Sema7A, and PCDH10 as the axon-sorting molecules for glomerular segregation. Genetic knockout (KO) experiments demonstrated that these molecules are involved in neural circuit formation in the mouse olfactory system (*22*, *25*, *33*) (fig. S1). The expression levels of these molecules are uniquely correlated with OR types (*22*, *24*, *27*). However, the expression patterns differed among glomeruli in the OB (Fig. 1A). For example, Kirrel2 expression was high in the I7 glomeruli but low in the MOR28 and M71 glomeruli. In contrast, PCDH10 expression was high in the M71 glomeruli, middle in the I7 glomeruli, and low in the MOR28 glomeruli (Fig. 1, B and C). Our previous study showed that the expression levels of these molecules dropped substantially to undetectable levels in KOs of the cyclic nucleotide–gated (CNG) channel (*27*), a key component of the olfactory signal transduction pathway (*34*). High-KCl treatment of olfactory tissues in ex vivo culture conditions increased the expression of these genes, and this effect was blocked by the depletion of extracellular calcium ions or inhibition of the voltage-gated L-type calcium channel (fig. S2). These results indicate that calcium influx associated with neural activity is required for generating the combinatorial code of the axon-sorting molecules.

Visualizing OSN spontaneous activity

To examine the nature of OSN spontaneous activity, we used a Cre/*loxP* approach [*pGoofy-Cre*: *pCAG-LSL-GCaMP6f* (*Ai95D*) mice] to express the genetically encoded calcium indicator GCaMP6f (*35*) specifically in OSNs (Fig. 2A). In the OSN-specific GCaMP6f mice, action potentials were reliably detected as transient increases in the fluorescence intensities of GCaMP6f (fig. S3). Correlation analyses revealed that spontaneous calcium events were not spatially or temporally correlated between OSNs in ex vivo acute olfactory epithelium (OE) slices from neonatal mice (Fig. 2, A and B; see also movie S1), which suggested that spontaneous calcium transients are sporadic events and occur independent of neighboring OSNs. These results are in contrast to the spontaneous activity patterns observed in the developing retina, which generates temporally correlated activity among neighboring retinal

[1]Laboratory of Chemical Pharmacology, Graduate School of Pharmaceutical Sciences, University of Tokyo, Tokyo 113-0033, Japan. [2]Laboratory for Animal Resource Development, RIKEN Center for Biosystems Dynamics Research, 2-2-3 Minatojima Minami-machi, Chuo-ku, Kobe 650-0047, Japan. [3]Laboratory for Genetic Engineering, RIKEN Center for Biosystems Dynamics Research, 2-2-3 Minatojima Minami-machi, Chuo-ku, Kobe 650-0047, Japan. [4]Center for Information and Neural Networks, National Institute of Information and Communications Technology, Suita City, Osaka 565-0871, Japan. [5]Social Cooperation Program of Evolutional Chemical Safety Assessment System, LECSAS, Graduate School of Pharmaceutical Sciences, University of Tokyo, Tokyo 113-0033, Japan.
*These authors contributed equally to this work.
†Corresponding author. Email: haruki-t@mol.f.u-tokyo.ac.jp

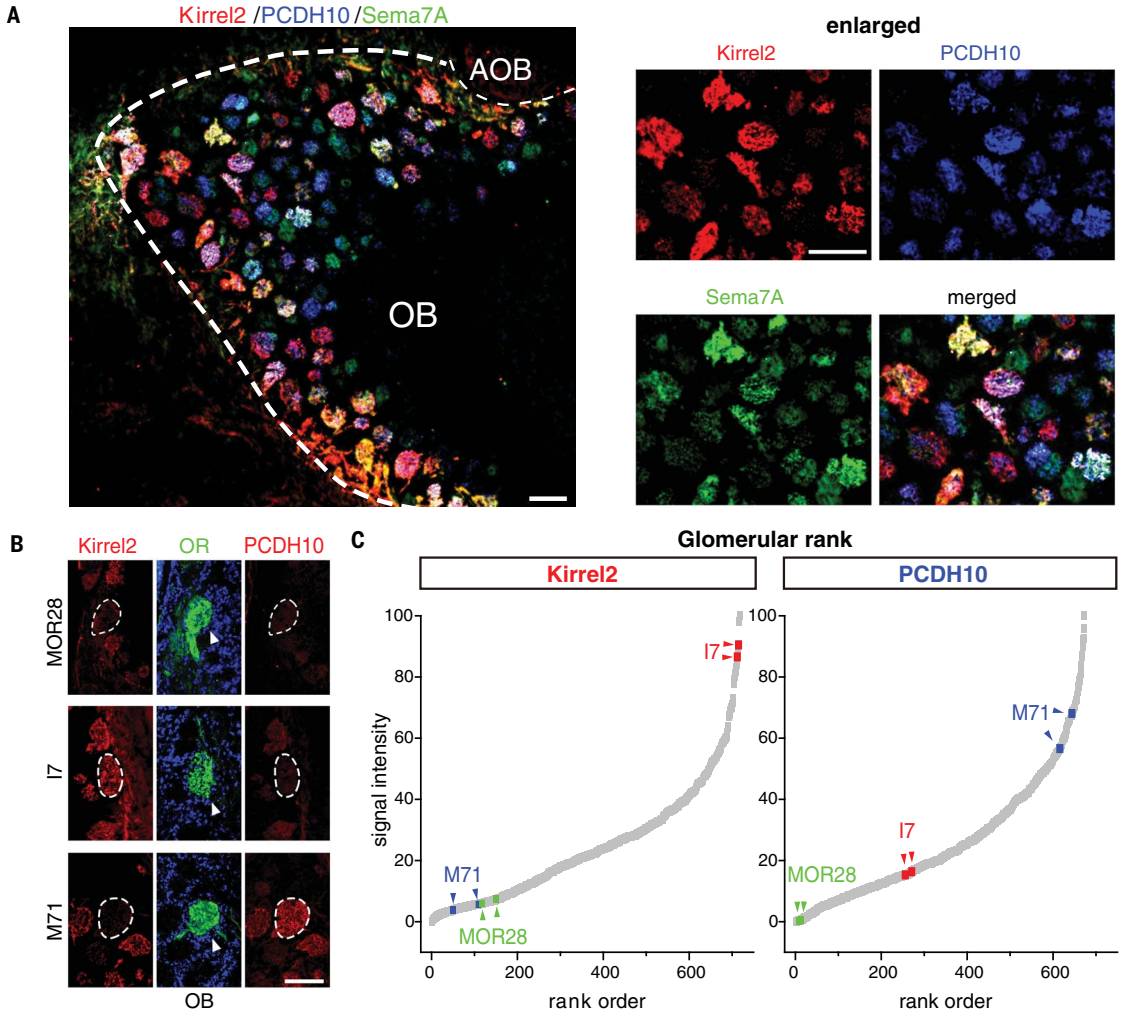

Fig. 1. OR-specific expression patterns of axon-sorting molecules. (**A**) Glomerulus-specific expression of axon-sorting molecules. A parasagittal OB section from a 2-week-old mouse was immunostained using antibodies to Kirrel2 (red), PCDH10 (blue), and Sema7A (green). Enlarged images are shown at the right. AOB, accessory olfactory bulb. Scale bars, 100 μm. (**B**) Expression levels of axon-sorting molecules in OSNs expressing specific ORs. The glomerular locations of MOR28-, I7-, and M71-expressing OSNs were identified by immunostaining with the indicated antibodies (indicated by arrowheads). Adjacent sections were immunostained using antibodies to Kirrel2 and PCDH10. Scale bars, 100 μm. (**C**) Rank order of expression levels of Kirrel2 and PCDH10. The signal intensities of Kirrel2 and PCDH10 were quantified for each glomerulus and plotted in order (N = 718 glomeruli for Kirrel2, N = 673 glomeruli for PCDH10).

ganglion cells and regulates precise circuit formation (*10*, *36*–*39*). In the CNG-KO mice, spontaneous activity was still present (*34*) (fig. S3E, see also movie S2) but in altered patterns; the event frequencies of calcium spikes and the inter-event intervals (IEIs) (frequency = 0.90 ± 1.02 times/min, IEI = 59.09 ± 61.52 s; mean ± SD, N = 230 cells) were lower and longer, respectively, relative to those in wild-type mice (frequency = 2.05 ± 2.48 times/min, IEI = 48.14 ± 53.09 s; mean ± SD, N = 252 cells). Because CNG channel–mediated activity is essential for the expression of *Kirrel2*, *Sema7A*, and *PCDH10* (*27*), these observations indicate that specific features of neural activity (e.g., frequency, IEI), rather than the presence of neural activity, are important for the expression of axon-sorting molecules, leading to the hypothesis that neural activity is instructive for glomerular segregation.

ORs determine spontaneous activity patterns

We next compared the temporal features of spontaneous calcium transients between OSNs expressing different OR types. We selected two types of OR-defined neurons based on the expression profiles of the axon-sorting molecules: (i) I7-expressing OSNs, in which expression levels of *Kirrel2* are high, and (ii) MOR28-expressing OSNs, in which expression levels of *Kirrel2* are low (Fig. 1, B and C, and fig. S4). We generated the transgenic mice *H-I7-Cre-mcherry* and *H-MOR28-Cre-mcherry* (hereafter abbreviated as *H-OR-Cre* lines), in which Cre recombinase was coexpressed with *I7* or *MOR28* (Fig. 2C and fig. S4). Because the forced expression of OR from a transgene suppresses endogenous OR expression (*6*, *40*, *41*), the monogenic OR expression is maintained in OSNs expressing the transgenes. The *H-OR-Cre* lines were then crossed with *Ai95D* mice to visualize spontaneous calcium transients of OSNs expressing specific ORs. We compared the features of calcium spikes, including baseline fluorescence, total event number, IEI, peak amplitude, coefficient of variation (CV), and rise and fall times of calcium spikes between I7- and MOR28-expressing neurons (N = 59 cells for I7, N = 61 cells for MOR28). We found that calcium transient patterns were significantly different between I7- and MOR28-expressing OSNs (Fig. 2C), even though both ORs were expressed under the control of the same *MOR23* promoter (*42*) (Fig. 2C and fig. S4A). I7-expressing OSNs exhibited calcium transients of higher amplitudes and higher frequencies than those of MOR28-expressing OSNs (Fig. 2, C and D). We conducted multidimensional scaling (MDS) to plot the datasets of I7- and MOR28-expressing OSNs according to relative distance (Fig. 2E). In the MDS space, OSNs expressing different ORs were significantly separated by a single line determined by the linear support vector machine (SVM) classifier (gray dashed line in Fig. 2E, F1 = 0.775, P < 0.0001), indicating that different ORs are sufficient to induce differing patterns of spontaneous calcium transients.

To overview a variety of calcium transient patterns in OSNs, we next collected the features of calcium transients from a large number of OSNs [N = 3214 cells; N = 59 for I7 (red), N = 61 for MOR28 (green), N = 45 for M71 (blue), and N = 3049 for randomly selected OSNs (gray)]. The dataset was dimension-reduced by principal components analysis (PCA). In two-dimensional PC space, OSNs were clustered depending on the expressed OR types (Fig. 2F and fig. S5). Taken together, this result indicates that OSNs expressing the same OR type exhibited similar temporal profiles of calcium transients.

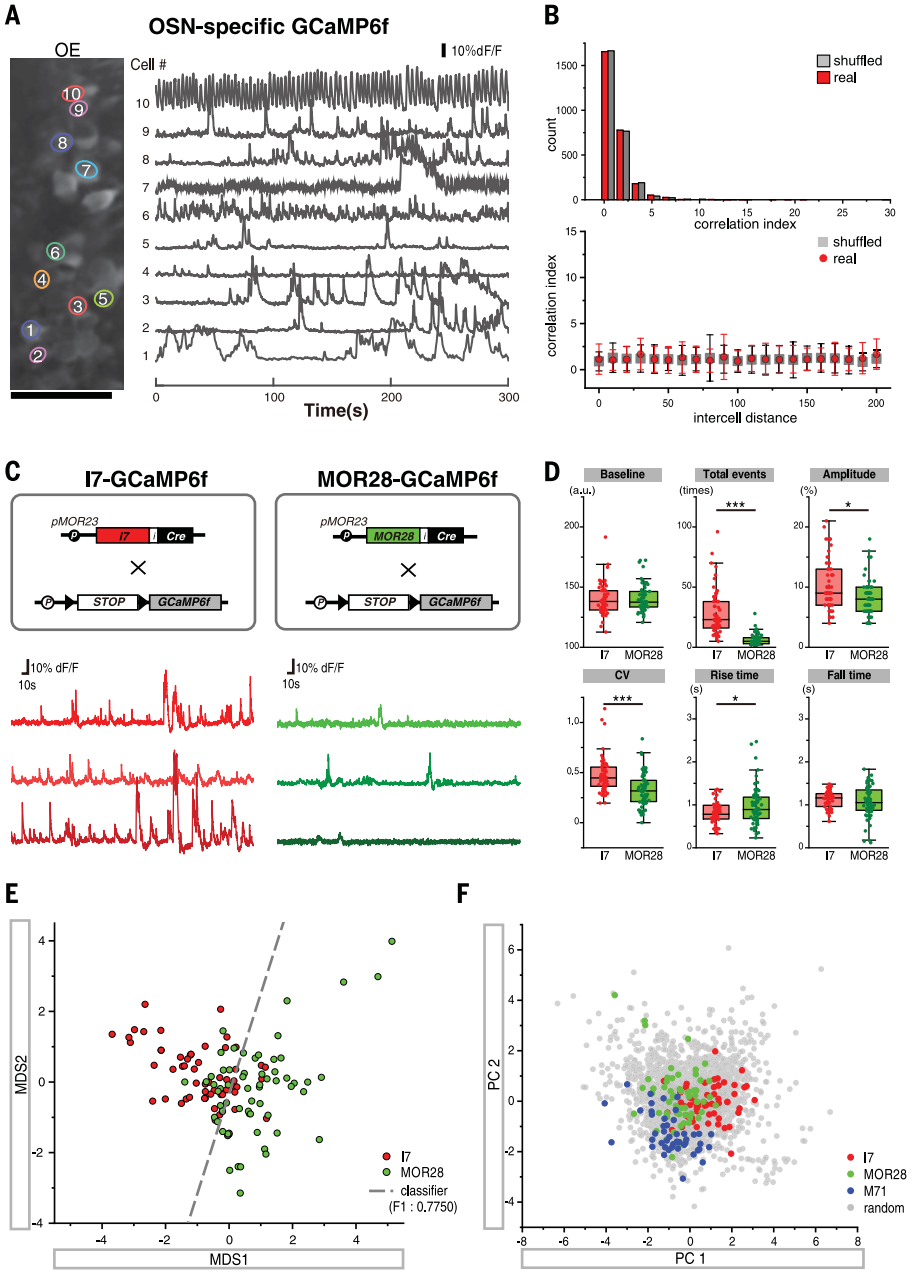

Fig. 2. Spontaneous activity patterns correlate with OR types. (**A**) An image of an OE acute slice. OSN calcium transients are shown at the right. Scale bar, 50 μm. (**B**) Pairwise cross-correlation analyses were performed for all possible pairs (N = 2701 pairs). Top: The distribution of the correlation indices for the real data was not significantly different from that for shuffled data (Mann-Whitney U test). Bottom: Correlation indices were plotted as a function of the intercell distance between cell pairs. Data are means ± SEM. (**C**) Top: *H-OR-Cre* lines were crossed with *Ai95D* mice. Bottom: Representative calcium transients. (**D**) Features of spontaneous calcium transients were analyzed for I7- or MOR28-expressing OSNs. Results are shown as box-and-whisker plots displaying the median and interquartile ranges. Outliers are 1.5 times the interquartile range (IQR) either above the third quartile or below the first quartile. CV, coefficient of variation. ***P < 0.001, *P < 0.05 (Mann-Whitney U test). (**E**) Multidimensional scaling (MDS) of the calcium imaging dataset of OR-defined OSNs. The support vector machine (SVM) classifier is shown as a gray dashed line. (**F**) PCA biplot of the calcium imaging dataset from 3214 OSNs.

Spike bursts increase *Kirrel2* expression

To assess the causal links between the neural activity patterns and the expression of axon-sorting molecules, we used an optogenetic approach to manipulate the neural activity of OSNs. OSN-specific channelrhodopsin-2 (ChR2) mice were generated by crossing *pGoofy-Cre* mice with *pCAG-LSL-ChR2* (*Ai32*) mice (*43*) (Fig. 3A, top). Blue light pulses (3 ms at ≤40 Hz) could precisely control the neural activity of OSNs at a single spike level, irrespective of the light power (fig. S6). The OSN-specific ChR2 mice were stimulated by blue light pulses with two different protocols, namely phasic burst stimulation (intraburst frequency, 10 Hz; action potentials in burst, 15; interburst interval, 15 s) and tonic stimulation (Fig. 3B). In both protocols, light-induced action potentials were maintained at the overall firing rate of 1 Hz because the median firing rate of the spontaneous activity of OSNs was 1.1 Hz (fig. S7). We illuminated the unilateral dorsolateral side of the OE with blue light pulses for 12 hours according to the protocols and compared the changes in the expression of axon-sorting molecules between the light-illuminated and shaded sides of the OE (Fig. 3A, bottom). We found that in the phasic burst protocol, *Kirrel2* was up-regulated in the light-stimulated side relative to the shaded side (Fig. 3B). However, no significant change was observed in the tonic protocol. *Kirrel2* expression was up-regulated in the phasic burst protocols when the interspike intervals (ISIs) of the induced spikes within bursts were less than 200 ms (Fig. 3C). Single-cell quantification further revealed that the intraburst frequency of the induced spikes had different impacts on *Kirrel2* up-regulation (ISI = 50 ms, d = 0.74; ISI = 100 ms, d = 1.54; ISI = 200 ms, d = 1.09) (Fig. 3D, left). *Kirrel2* expression increased even in MOR28-expressing OSNs, where the endogenous *Kirrel2* expression levels are low (Fig. 3D, right), indicating that the change in the expression levels of *Kirrel2* was not attributable to a difference in the OSN population. In addition, the induced spike numbers within bursts affected *Kirrel2* expression (Fig. 3E).

To find the relationship between endogenous spontaneous activity and optogenetically induced firing, we conducted SVM classification in terms of *Kirrel2* expression levels. The nonlinear SVM classifier based on endogenous activity patterns of *Kirrel2*-high (I7) and *Kirrel2*-low (MOR28 and M71) OSNs could predict the light stimulation–induced *Kirrel2* up-regulation (Fig. 3F, left). The optogenetic stimulation protocols that increased *Kirrel2* expression (Fig. 3F, a to d) were plotted onto the *Kirrel2*-high side of the graph, whereas those that did not change *Kirrel2* expression (Fig. 3F, e to g) were plotted onto the *Kirrel2*-low side. Further, OSNs in the I7 cluster frequently exhibited calcium transients with high amplitude that resembled phasic burst stimulation (Fig. 3F, right, calcium event frequency = 0.047 ± 0.031 Hz, calcium event amplitude = 10.25 ± 4.06%, mean ± SD). In contrast, such high-amplitude calcium transients were not frequently observed in the MOR28 and M71 clusters (MOR28, frequency = 0.011 ± 0.008 Hz, amplitude = 8.28 ± 2.98%, mean ± SD; M71, frequency = 0.036 ± 0.033 Hz, amplitude = 4.11 ± 1.17%, mean ± SD). Thus, we deduced that the phasic burst stimulations mimicked the physiological patterns of neural activity for *Kirrel2* expression.

In contrast to *Kirrel2*, the expression of *Sema7A* and *PCDH10* did not change during the series of experiments (Fig. 3C). A similar phenotype was also observed in the CNG-KO background, where

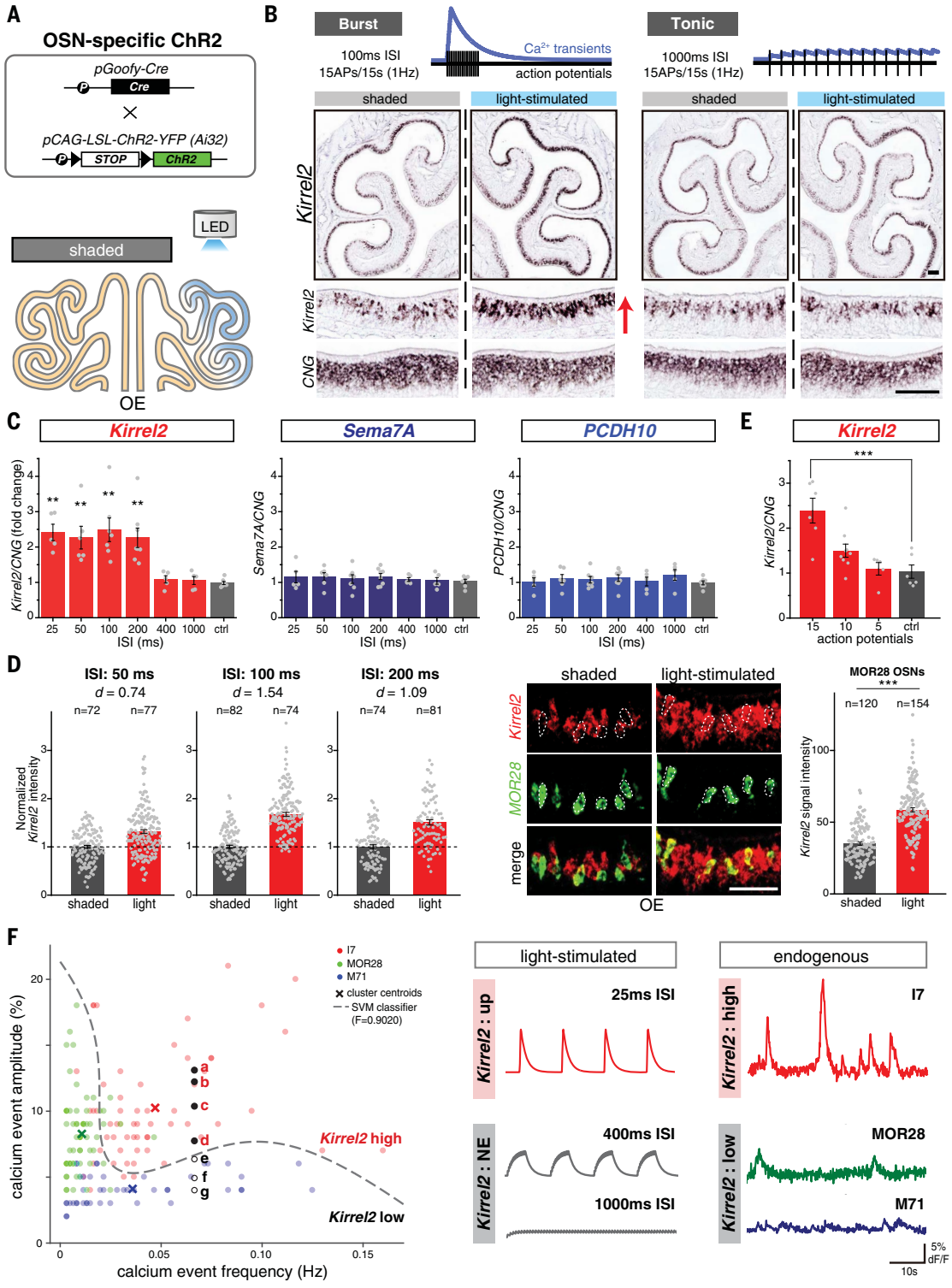

Fig. 3. Phasic burst stimulation increases *Kirrel2* expression. (**A**) Top: Transgenic constructs for the OSN-specific ChR2 mice. Bottom: Experimental schematic for the in vivo optogenetic stimulation. (**B**) In situ hybridization of the OE sections using probes for *Kirrel2* and *CNG* channel (mature OSN marker). (**C**) Relative expression levels of axon-sorting molecules were compared by quantitative RT-PCR; $N = 5$ to 8 mice per group. (**D**) Left: Single-cell analyses of gene expression changes. Right: Relative *Kirrel2* signal intensities in MOR28-expressing OSNs. $^{***}P < 0.001$ (Student *t* test). (**E**) Differential impacts of *Kirrel2* by protocols comprising different spike numbers. Relative *Kirrel2* levels were compared by quantitative RT-PCR; $N = 5$ to 9 mice per group. $^{**}P < 0.01$, $^{***}P < 0.001$ [one-way analysis of variance (ANOVA) with post hoc Tukey test in (C) and (E)]. Error bars in (C) to (E) denote SEM. (**F**) Left: Scatterplot of the calcium imaging data. The SVM classifier divides OSNs according to *Kirrel2* levels (gray dashed line). The expected calcium transients through light stimulation are also plotted: **a**, 25 ms ISI, 15 APs, 15 s; **b**, 50 ms ISI, 15 APs, 15 s; **c**, 100 ms ISI, 15 APs, 15 s; **d**, 200 ms ISI, 15 APs, 15 s; **e**, 400 ms ISI, 15 APs, 15 s; **f**, 200 ms ISI, 10 APs, 15 s; **g**, 200 ms ISI, 5 APs, 15 s. Right: Calcium transients nearest to the centroids of each OR cluster are compared with the expected calcium transients induced by light stimulation. NE, no effect. See also fig. S11. Scale bars, 50 μm.

endogenous calcium transients were more static (fig. S8). These results demonstrate that the spike bursts specifically up-regulate *Kirrel2* expression.

Prolonged burst stimulation increases *Sema7A* and *PCDH10*

We next sought to determine which pattern of neural activity was necessary for the expression of *Sema7A* and *PCDH10*. Because they showed similar protein distribution patterns at the OSN axon termini (27), there must be a common regulatory mechanism underlying their expression. We stimulated OSNs with various burst duration protocols ranging from 1.5 to 720 s (Fig. 4A). We kept the overall firing rate at 1 Hz and the spike frequency within bursts at 10 Hz. Optogenetic stimulation with various burst duration protocols revealed that *Sema7A* and *PCDH10* were up-regulated by burst durations for more than 10 s and 20 s, respectively (Fig. 4B). It is notable that the 360-s and 720-s burst duration protocols increased the expression of *Sema7A* and *PCDH10*, but not that of *Kirrel2* (Fig. 4, B and C).

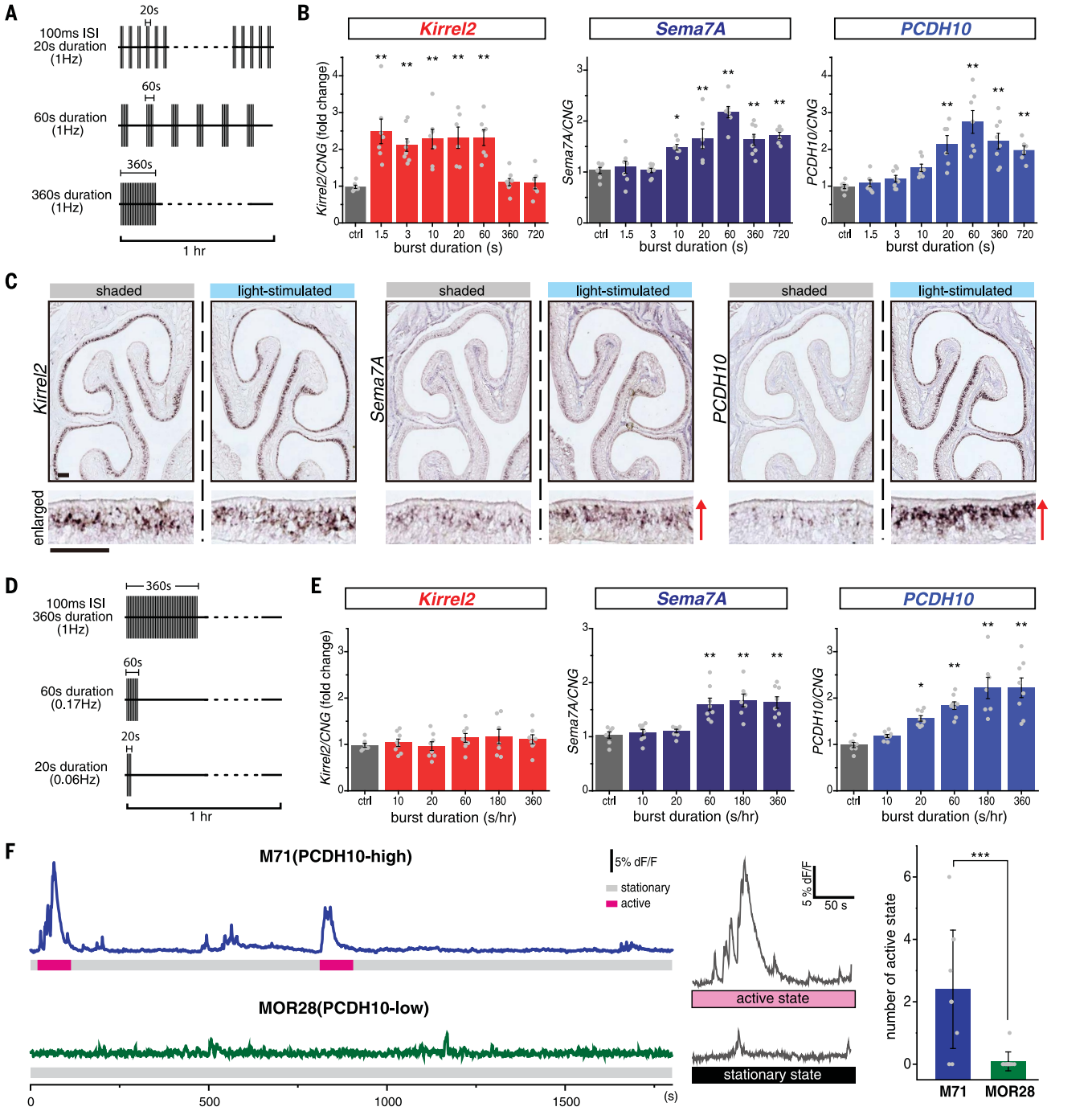

Fig. 4. Prolonged burst stimulation increases *Sema7A* and *PCDH10*. (**A**) Schematic showing various stimulation protocols. (**B**) Expression changes of axon-sorting molecules upon different light stimulation protocols. Quantitative analyses were performed as in Fig. 3C. Error bars denote SEM (N = 6 to 8 mice per group). (**C**) In situ hybridization of the OE sections from OSN-specific ChR2 mice illuminated by blue light with the long-duration protocol (ISI, 100 ms; burst duration per hour, 360 s). Enlarged photos are shown at the bottom. Scale bars, 50 μm. (**D**) Schematic showing various optogenetic stimulation protocols. (**E**) Expression changes of axon-sorting molecules upon various burst units. Quantitative analyses were performed as in Fig. 3C. Error bars denote SEM (N = 7 or 8 mice per group). $^{*}P < 0.05$, $^{**}P < 0.01$ [one-way ANOVA with post hoc Tukey test in (B) and (E)]. (**F**) Left: Long-term calcium imaging of *PCDH10*-high (M71) and *PCDH10*-low (MOR28) OSNs. Right: Number of active states per hour in M71- and MOR28-expressing OSNs. Data are means ± SD. N = 10 cells (M71), 11 cells (MOR28). $^{***}P < 0.001$ (Student t test).

To investigate the minimum duration of bursts required for the expression of *Sema7A* and *PCDH10*, we further tested the effects of various burst units by changing the burst duration irrespective of the firing rate of the induced spikes (Fig. 4D). To this end, OSNs were stimulated hourly with various types of single burst units (intraburst frequency, 10 Hz; burst duration, 10 to 360 s) for 12 hours. We found that both genes were up-regulated by prolonged bursts. The sensitivities to the burst duration differed between *Sema7A* and *PCDH10*; a 20-s burst duration induced the expression of *PCDH10*, but not that of *Sema7A* (Fig. 4E). The differential sensitivities of *Sema7A* and *PCDH10* to the burst durations may

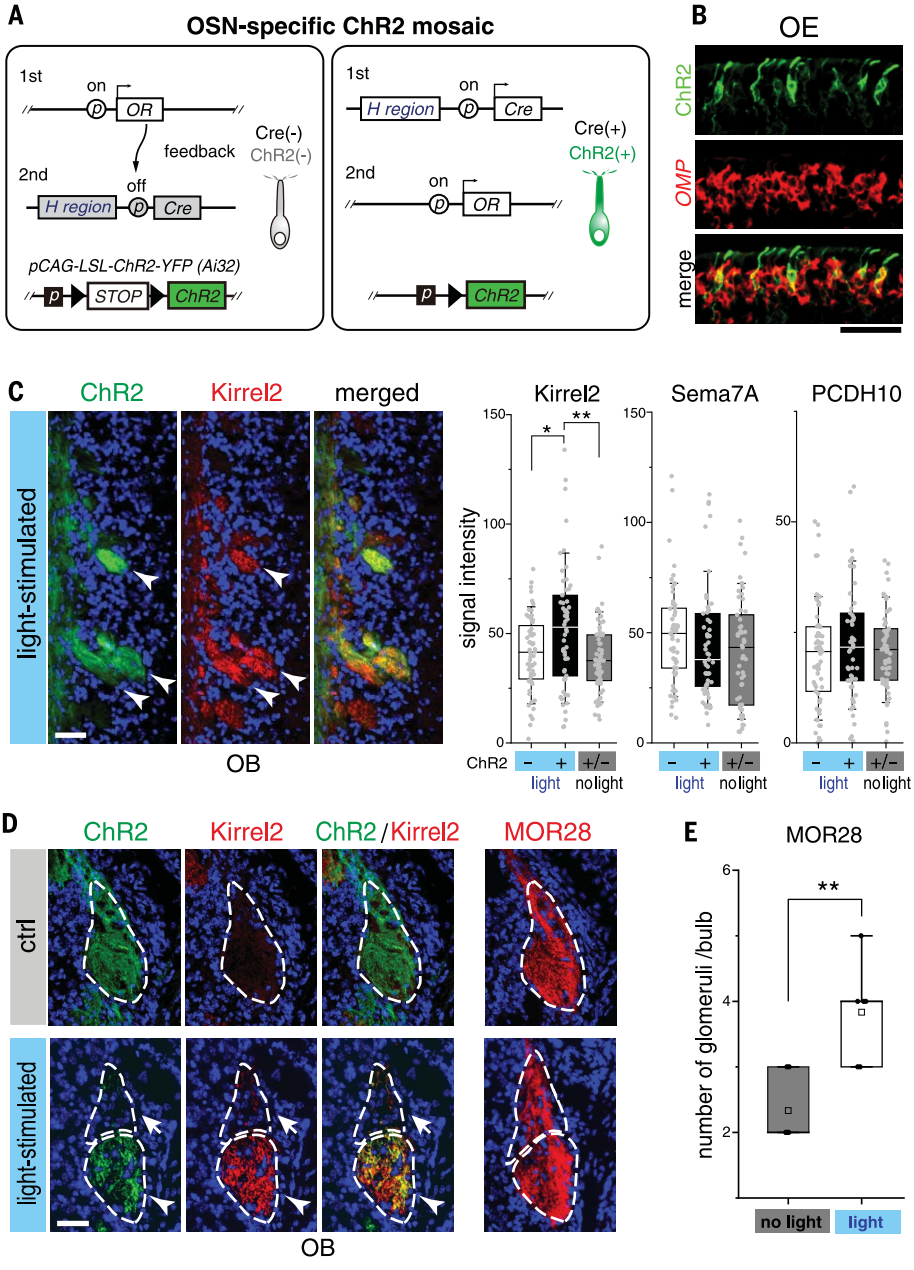

Fig. 5. Optogenetic stimulation affects axonal segregation. (**A**) Schematic for generating OSN-specific ChR2 mosaic mice. (**B**) Double staining of an OE section from the ChR2 mosaic mouse. An OE section was subjected to in situ hybridization using an *OMP* probe (red) and immunostaining with antibodies to green fluorescent protein (GFP) (green). (**C**) Immunostaining of an OB section with antibodies to GFP and Kirrel2 after chronic light stimulation (intraburst frequency, 10 Hz; APs within burst, 15; interburst interval, 15 s). Left: Kirrel2 up-regulation upon light stimulation is indicated by arrowheads. Right: Quantification of protein levels of axon-sorting molecules. $*P < 0.05$, $**P < 0.01$ (one-way ANOVA with post hoc Tukey test). See also data S5. (**D**) Immunostaining of OB sections using antibodies to Kirrel2, GFP, and MOR28. Kirrel2-positive and -negative MOR28^{+} axons are indicated by arrowheads and arrows, respectively. (**E**) Numbers of MOR28 glomeruli per OB in ChR2 mosaic mice with and without light stimulation. A glomerular structure was semiautomatically defined by immunofluorescence signals of vesicular glutamate transporter2 (VGlut2). Box and whiskers in all graphs represent 25th to 75th and 10th to 90th percentiles, respectively. Scale bars, 50 μm. $N = 6$ glomeruli, $**P < 0.01$ (Student t test).

explain their partially overlapping but different expression patterns in the OSN axon termini in the OBs (*27*). In a series of burst duration experiments (Fig. 4D), *Kirrel2* expression was not changed (Fig. 4E). These results indicate that *Sema7A* and *PCDH10* expression is up-regulated by protocols of low-frequency and long-duration bursts, whereas *Kirrel2* expression is up-regulated by protocols of high-frequency and short-duration bursts.

We also performed long-term calcium imaging for OSNs expressing *M71* and *MOR28* in which *PCDH10* expression levels are high and low, respectively (Fig. 1, B and C). As shown in Fig. 4F, both types of OSNs exhibited stationary states during the majority of the recorded time. However, we observed events of prolonged calcium elevation several times per hour in M71-expressing OSNs (Fig. 4F). We defined the active state according to the duration when OSNs showed a higher amplitude of calcium transients above average for >20 s. The active state in M71-expressing OSNs lasted for 34.14 ± 13.47 s with an IEI of 445.85 ± 376.03 s (mean ± SD), which is enough to induce *PCDH10* expression. In contrast, the active state was hardly observed in MOR28-expressing OSNs [0.09 ± 0.30 times/hour (N = 11 cells) versus 2.4 ± 1.90 times/hour for *M71*-expressing OSNs (N = 10 cells), means ± SD]. These results suggest that prolonged burst stimulations and their impact on gene expression mimicked physiological conditions.

Chronic optogenetic stimulation induces axonal segregation

To examine whether in vivo optogenetic stimulation indeed affects segregation of OSN axons, we conducted optogenetic stimulation for a prolonged period of time. For this purpose, we used *H-Cre* transgenic mice (*13*). In this mouse, Cre recombinase is expressed in a subset of OSNs as a result of the OR-mediated negative feedback signal (*6*). Therefore, ChR2-positive and ChR2-negative OSNs expressing the same OR can be generated in the same individuals by crossing the *H-Cre* transgenic mice with the *Ai32* mice (Fig. 5, A and B).

Neonatal OSN-specific ChR2 mosaic mice were stimulated for 5 to 6 hours per day with the phasic burst protocol used in Fig. 3B. After 1 week of light stimulation, we observed an increase in Kirrel2 proteins, but not in PCDH10 or Sema7A proteins, in ChR2-positive OSN axons (Fig. 5, C and D). The Kirrel2 up-regulation was also observed in the CNG-KO background where endogenous Kirrel2 expression is decreased (fig. S9). We found segregation of MOR28-expressing OSN axons according to ChR2 expression in the OB of the ChR2 mosaic mice (Fig. 5, D and E). A similar axonal phenotype was also found in I7-expressing OSN axons (fig. S10, A and B). The ChR2-dependent axonal segregation did not occur without light stimulation (Fig. 5, D and E, and fig. S10). These results indicate that the optogenetically induced phasic burst stimulation induced axonal segregation, presumably through Kirrel2 up-regulation.

Discussion

Hebbian plasticity explains the activity-dependent development of many neural circuits (*19*). Synchronous firing of presynaptic neurons, such as retinal waves in the visual system (*2*, *36*, *37*, *39*, *44*, *45*), is a prerequisite for the Hebbian plastic changes. In the present study, we did not observe spatial or temporal correlations for the spontaneous activities among OSNs (Fig. 2, A and B). Rather,

spontaneous activity patterns of OSNs were uniquely correlated with OR types. We also showed that differing neural activity patterns induced the expression of different axon-sorting molecules regulating axonal segregation. On the basis of these results, we propose an activity-dependent mechanism, different from the Hebbian plasticity theory, in which specific patterns of spontaneous activity determined by the expressed ORs contribute to generate the combinatorial code of axon-sorting molecules for OR-specific glomerular segregation.

Our calcium imaging analyses in OR substitution experiments demonstrated that ORs determine spontaneous activity patterns. How are spontaneous activity patterns regulated by ORs? It has been reported that G protein–coupled receptors (GPCRs), including ORs, produce unique levels of basal cAMP (cyclic adenosine monophosphate) in a ligand-independent manner (*12*, *46*, *47*). A plausible explanation is that the OR-derived basal activity contributes to the pattern of spontaneous activity. However, mutations of a GPCR that result in altered basal cAMP levels do not affect the expression of axon-sorting molecules in OSNs (*12*). Therefore, the OR-derived basal activity is unlikely to be a determinant of spontaneous activity patterns. In this study, we found that individual OSNs show different firing patterns in response to continuous optogenetic stimulation (fig. S6D). Moreover, several voltage-dependent calcium channels and transient receptor potential channels are expressed in a subset of OSNs (*48*–*51*). It is possible that the intrinsic membrane properties vary among OSNs expressing different OR types for OR-correlated patterns of spontaneous activity. However, the mechanisms linking the membrane properties to expressed ORs remain unknown.

In this study, we demonstrated the firing pattern–dependent expression of axon-sorting molecules by optogenetic stimulation. The SVM classification indicated that optogenetic stimulation experiments mimicked physiological conditions (Fig. 3F and fig. S11). We found that phasic, repetitive short bursts of neural activity induced *Kirrel2* expression, whereas prolonged durations of bursting activity induced the expression of *Sema7A* and *PCDH10*. Increased levels of *Kirrel2* were dependent on spike numbers and ISIs within bursts in the phasic burst stimulation (Fig. 3, D and E). The sensitivities to the burst duration might differ between *PCDH10* and *Sema7A*. We observed statistically significant up-regulation of *PCDH10* and *Sema7A* by burst durations of >20 s and >60 s, respectively (Fig. 4E). This firing pattern–dependent expression allows OSNs to separately regulate the types and levels of axon-sorting molecules to generate the combinatorial code for glomerular segregation (fig. S12).

How do OSNs decode the temporal patterns of their own neural activity into diverse expression of axon-sorting molecules? Previous studies have identified transcription factors that are activated by different patterns of calcium transients (*52*–*54*). For example, CaMKII (calcium/calmodulin-dependent protein kinase II) is activated by high-frequency calcium oscillations, whereas NFATs (nuclear factors of activated T cells) are activated by low-frequency oscillations (*55*). The differential properties (e.g., sensitivity, affinity, and kinetics) of calcium-responsive factors may provide a molecular basis for the differential readouts of neural activity patterns.

In the nervous system, neural activity is involved in various aspects of the neural development and plasticity—including cell type specification, dendritic branching, synaptic maturation, and learning and memory—through a complex program of gene regulation (*56*–*59*). Although several hundreds of genes have been identified as activity-dependent genes (*60*), their regulatory mechanisms and functions are not fully understood. In this study, we demonstrated firing pattern–dependent gene expression regulating neural circuit formation. With this strategy, neurons can generate variation through diversifying gene expression with only a single second messenger. The pattern-dependent regulation may also expand beyond development to the plasticity of neural circuits, which is the basis for learning and adapting to environmental changes throughout the lifetime.

Materials and methods

Mutant mice

All experimental procedures were performed with the approval of the animal experiment ethics committee of the University of Tokyo and Institutional Animal Care and Use Committee (IACUC) of RIKEN Kobe Branch, and in accordance with the guidelines for the care and use of laboratory animals of the University of Tokyo and RIKEN Kobe Branch. *H-Cre* mice were as described (*13*). *Ai95D*, *Ai32*, *M71-ires-Cre*, and CNG-KO mice were purchased from the Jackson Laboratory. *pGoofy-Cre* and *Kirrel2* conditional KO (RBRC06340) mice were generous gifts provided by Y. Yoshihara and H. Sakano, respectively. To generate the *H-I7* (accession no. CDB0537T: www2.clst.riken.jp/arg/TG%20mutant%20mice%20list.html) and *H-MOR28* (accession no. CDB0536T: www2.clst.riken.jp/arg/TG%20mutant%20mice%20list.html) minigene constructs, a 10.1-kb *Sac*I fragment containing the *MOR23* gene from a BAC clone of a C57BL/6 mouse (RP23-306I18) was subcloned into pBluescript II SK(+). The 2.1-kb *H enhancer* fragment (*22*) was attached to the 5′ end of the MOR23 minigene and an *ires-Cre-ires-mcherry* fragment was inserted into the 3′-UTR of the minigene. The 930-bp coding sequence of *MOR23* was replaced with that of *I7* or *MOR28*. The transgene sequences were excised by *Asc*I digestion, separated from the vector DNA by sucrose gradient centrifugation, and then microinjected into the pronuclei of CD-1 embryos.

Immunostaining and in situ hybridization

Immunostaining was performed largely as described (*22*). Mice were anesthetized with sodium pentobarbital (2.5 mg/animal) and perfused intracardially with 4% paraformaldehyde in phosphate-buffered saline (PBS). The olfactory bulb (OB) was embedded briefly in an optimal cutting temperature (OCT) compound (Tissue-Tek; Sakura Finetek) in liquid nitrogen. The olfactory epithelium (OE) was dissected and fixed overnight with 4% paraformaldehyde in PBS and decalcified in 0.5 M ethylenediaminetetraacetic acid for 8 to 10 hours at 4°C. Tissues were then incubated in 30% sucrose overnight at 4°C and embedded in an OCT compound in liquid nitrogen. Serial sections (10 μm for the OE, 12 μm for the OB) were prepared with CM3050 cryostat (Leica) and collected onto Matsunami adhesive silane-coated glass slides (Matsunami Glass). Slides were rinsed with PBS three times and incubated in a blocking buffer [5% skim milk in PBS with 0.2% Triton X-100 (PBST)] for 1 hour at room temperature (RT). After the blocking, the slides were incubated with primary antibodies overnight at RT. After being washed with PBST three times, the sections were treated with secondary antibodies (Molecular Probes) at a dilution of 1:400. The primary antibodies used in this study are listed in data S7. The VectaStain ABC Kit (Vector Laboratories Inc.) was used to obtain higher intensity in the immunostaining of ORs. In situ hybridization was performed as described (*13*). The sequences of the RNA probes that were used are listed in data S7. The full-length coding sequence for *mcherry* was subcloned into the pGEM-T vector (Promega) and used as a template.

Signal intensity measurement and statistical analysis

Optical and fluorescent images of sections were obtained using a BZ-X700 microscope (Keyence). A glomerular structure was defined by immunofluorescence signals of vesicular glutamate transporter2 (VGlut2), and staining intensities of Kirrel2, Sema7A, and PCDH10 within glomerulus were measured using ImageJ (NIH). After subtracting the background signals, staining intensities were divided by the highest staining intensity and were normalized to 100% (Fig. 1C). In Fig. 3D, signal intensities were rescaled such that the rescaled mean in the shaded side is 1. The data are presented as means ± SEM.

Optogenetic stimulation

Mice were placed on ice to anesthetize them by hypothermia and a skin incision was made over the dorsal surface of the head. Xylocaine jelly (2%, AstraZeneca) was applied to the bone overlying the OE as a local anesthetic, and a cover slip was placed over the bone to prevent the olfactory tissue from drying out. The olfactory sensory neurons (OSNs) were stimulated using 470-nm LEDs (Lex2; Brain Vision LLC). To stimulate the OE unilaterally, LEDs were placed directly outside the right side of the OE, whereas the other side was covered with thin aluminum to avoid light stimulation. After 12 hours of stimulation, the glass cover was removed from the skull and olfactory tissues were collected for reverse transcription polymerase chain reaction (RT-PCR) or in situ hybridization. For chronic stimulation, pups were wrapped tightly in gauze bandage

before stimulation and placed in an acrylic chamber. Blue LEDs were placed directly outside the dorsal side of the OE. After stimulation, pups were placed on a temperature-controlled heating pad before they were returned to their mothers. In all protocols, the light pulse duration was 3 ms with a power of 3 mW mm^{-2}. The timing, duration, and cycle of LED light stimulation were controlled with a pulse stimulator (Nihon Kohden).

RT-PCR

Quantitative PCR was performed as described (*13*). The expression levels of *Kirrel2*, *Sema7A*, and *PCDH10* were normalized to that of *CNG*. Primer sets and TaqMan probes used in this study were designed by Universal Probe Library (Roche) and Nihon Gene Research Laboratories Inc. (Miyagi). The primers and probe sequences used for RT-PCR are listed in data S7.

Slice preparation

Acute slices were prepared from neonatal mice (PD3-6). Mice were anesthetized and decapitated, and the olfactory tissue was embedded in 5% low-melting agar in Ringer's solution (125 mM NaCl, 2.5 mM KCl, 2 mM $CaCl_2$, 2 mM $MgCl_2$, 25 mM $NaHCO_3$, 10 mM HEPES, and 10 mM glucose) and cut into 200- to 300-μm-thick slices using a vibratome (Leica VT1200S) in ice-cold oxygenated artificial cerebrospinal fluid (aCSF; 125 mM NaCl, 2.5 mM KCl, 1 mM $MgCl_2$, 2 mM $CaCl_2$, 1.25 mM NaH_2PO_4, 25 mM $NaHCO_3$, and 10 mM glucose). Slices were briefly transferred to an interface chamber containing oxygenated artificial cerebrospinal fluid (aCSF) at RT.

Ex vivo culture

For ex vivo culture experiments, mice were anesthetized by hypothermia and were quickly decapitated. The nose was dissected en bloc to prepare intact septal nasal cartilage with epithelia. Samples were briefly transferred to an interface chamber containing oxygenated aCSF and were incubated at 35°C for 6 hours. After the incubation, OE samples were postfixed overnight with 4% paraformaldehyde in PBS.

Electrophysiological recording

Loose-patch recording was performed largely as described (*60*). Briefly, after anesthesia was achieved by hypothermia, mice were quickly decapitated, and the nose was dissected en bloc to prepare intact OE. The septal nasal cartilage with epithelia was placed in a submerged recording chamber with the mucus layer facing up and was continuously perfused with oxygenated aCSF at 35°C. For extracellular recording, pipettes with resistance of 4 to 8 MΩ were fabricated using the P-1000 micropipette puller (Sutter Instrument) and filled with aCSF. All recordings were performed using the Olympus BX51W0-I microscope. A 40× objective lens (0.8 numerical aperture, LUMplan FN; Olympus) was used to guide a patch pipette to individual OSNs. Recordings were performed in a loose patch configuration. A loose seal (resistance, 40 to 200 MΩ) was formed by applying gentle suction when an electrode tip contacted an OSN. Signals were band-filtered between 200 Hz and 5 kHz.

Calcium imaging and data analysis

Calcium imaging was conducted using acute slices of OE from mice expressing GCaMP6f. OE slices were placed in a recording chamber perfused with aCSF at 3 to 4 ml/s. Fluorophores were excited at 488 nm and visualized using a 507-nm long-pass emission filter. Videos were recorded at 10 frames/s for 10 min or 5 frames/s for 1 hour using a 40× water immersion objective lens (0.8 numerical aperture, CFI Apo 40XW NIR; Nikon), a Nipkow-disk confocal microscope (CSU-X1; Yokogawa Electric), and a cooled electron multiplying charge-coupled device camera (iXon DU897; Andor Technologies). Image acquisition was controlled by Andor Solis (Andor Technologies). The fluorescence change was measured as $(F_t - F_0)/F_0$, where F_t is the fluorescence intensity at a given time point and F_0 is the baseline. Automated quantification of the features of calcium transients was performed using FluoroSNNAP software (*61*). Principal components analyses were performed with Origin Pro (OriginLab). Multidimensional scaling (MDS) and support vector machine (SVM) classification were performed with MATLAB software. F1 score was calculated as a measure of the accuracy in the SVM classification (*62*).

Correlation analysis

To quantify the correlation between pairs of recorded cells, the correlation index (CI) was calculated as described (*33*, *40*). The formula was as follows:

$$\mathrm{CI} = \frac{N_{AB(-\Delta t,+\Delta t)}\,T}{N_{A(0,T)}N_{B(0,T)}\,2\Delta t}$$

where $N_{AB(-\Delta t,+\Delta t)}$ is the number of spikes from cell B that fall within $\pm\Delta t$ of any spike from A, T is the duration of the recording in seconds, and $N_{A(0,T)}$ and $N_{B(0,T)}$ are the total numbers of spikes detected from cells A and B during the recording. To evaluate the significance of deviations from the "random" baseline of the CI, surrogate data were generated through the random shuffling of real data. The spike coincidence time window in Fig. 2 was $\pm\Delta t$ = 200 ms.

REFERENCES AND NOTES

1. L. C. Katz, C. J. Shatz, Synaptic activity and the construction of cortical circuits. *Science* **274**, 1133–1138 (1996). doi: 10.1126/science.274.5290.1133; pmid: 8895456
2. L. A. Kirkby, G. S. Sack, A. Firl, M. B. Feller, A role for correlated spontaneous activity in the assembly of neural circuits. *Neuron* **80**, 1129–1144 (2013). doi: 10.1016/j.neuron.2013.10.030; pmid: 24314725
3. L. I. Zhang, M. M. Poo, Electrical activity and development of neural circuits. *Nat. Neurosci.* **4**, 1207–1214 (2001). doi: 10.1038/nn753; pmid: 11687831
4. L. Buck, R. Axel, A novel multigene family may encode odorant receptors: A molecular basis for odor recognition. *Cell* **65**, 175–187 (1991). doi: 10.1016/0092-8674(91)90418-X; pmid: 1840504
5. A. Chess, I. Simon, H. Cedar, R. Axel, Allelic inactivation regulates olfactory receptor gene expression. *Cell* **78**, 823–834 (1994). doi: 10.1016/S0092-8674(94)90562-2; pmid: 8087849
6. S. Serizawa *et al*., Negative feedback regulation ensures the one receptor–one olfactory neuron rule in mouse. *Science* **302**, 2088–2094 (2003). doi: 10.1126/science.1089122; pmid: 14593185
7. K. J. Ressler, S. L. Sullivan, L. B. Buck, Information coding in the olfactory system: Evidence for a stereotyped and highly organized epitope map in the olfactory bulb. *Cell* **79**, 1245–1255 (1994). doi: 10.1016/0092-8674(94)90015-9; pmid: 7528109
8. P. Mombaerts *et al*., Visualizing an olfactory sensory map. *Cell* **87**, 675–686 (1996). doi: 10.1016/S0092-8674(00)81387-2; pmid: 8929536
9. R. Vassar *et al*., Topographic organization of sensory projections to the olfactory bulb. *Cell* **79**, 981–991 (1994). doi: 10.1016/0092-8674(94)90029-9; pmid: 8001145
10. L. Luo, J. G. Flanagan, Development of continuous and discrete neural maps. *Neuron* **56**, 284–300 (2007). doi: 10.1016/j.neuron.2007.10.014; pmid: 17964246
11. H. Sakano, Neural map formation in the mouse olfactory system. *Neuron* **67**, 530–542 (2010). doi: 10.1016/j.neuron.2010.07.003; pmid: 20797531
12. A. Nakashima *et al*., Agonist-independent GPCR activity regulates anterior-posterior targeting of olfactory sensory neurons. *Cell* **154**, 1314–1325 (2013). doi: 10.1016/j.cell.2013.08.033; pmid: 24034253
13. H. Takeuchi *et al*., Sequential arrival and graded secretion of Sema3F by olfactory neuron axons specify map topography at the bulb. *Cell* **141**, 1056–1067 (2010). doi: 10.1016/j.cell.2010.04.041; pmid: 20550939
14. H. Takeuchi, H. Sakano, Neural map formation in the mouse olfactory system. *Cell. Mol. Life Sci.* **71**, 3049–3057 (2014). doi: 10.1007/s00018-014-1597-0; pmid: 24638094
15. C. R. Yu *et al*., Spontaneous neural activity is required for the establishment and maintenance of the olfactory sensory map. *Neuron* **42**, 553–566 (2004). doi: 10.1016/S0896-6273(04)00224-7; pmid: 15157418
16. A. S. Mobley *et al*., Hyperpolarization-activated cyclic nucleotide-gated channels in olfactory sensory neurons regulate axon extension and glomerular formation. *J. Neurosci.* **30**, 16498–16508 (2010). doi: 10.1523/JNEUROSCI.4225-10.2010; pmid: 21147989
17. T. Ishii *et al*., Monoallelic expression of the odourant receptor gene and axonal projection of olfactory sensory neurones. *Genes Cells* **6**, 71–78 (2001). doi: 10.1046/j.1365-2443.2001.00398.x; pmid: 11277098
18. P. Feinstein, P. Mombaerts, A contextual model for axonal sorting into glomeruli in the mouse olfactory system. *Cell* **117**, 817–831 (2004). doi: 10.1016/j.cell.2004.05.011; pmid: 15186781
19. D. O. Hebb, *The Organization of Behavior: A Neuropsychological Theory* (Wiley, 1949).
20. A. Bulfone *et al*., An olfactory sensory map develops in the absence of normal projection neurons or GABAergic interneurons. *Neuron* **21**, 1273–1282 (1998). doi: 10.1016/S0896-6273(00)80647-9; pmid: 9883721
21. J. A. St. John, H. J. Clarris, S. McKeown, S. Royal, B. Key, Sorting and convergence of primary olfactory axons are independent of the olfactory bulb. *J. Comp. Neurol.* **464**, 131–140 (2003). doi: 10.1002/cne.10777; pmid: 12898607
22. S. Serizawa *et al*., A neuronal identity code for the odorant receptor-specific and activity-dependent axon sorting. *Cell* **127**, 1057–1069 (2006). doi: 10.1016/j.cell.2006.10.031; pmid: 17129788
23. T. Cutforth *et al*., Axonal ephrin-As and odorant receptors: Coordinate determination of the olfactory sensory map. *Cell* **114**, 311–322 (2003). doi: 10.1016/S0092-8674(03)00568-3; pmid: 12914696
24. T. Kaneko-Goto, S. Yoshihara, H. Miyazaki, Y. Yoshihara, BIG-2 mediates olfactory axon convergence to target glomeruli. *Neuron* **57**, 834–846 (2008). doi: 10.1016/j.neuron.2008.01.023; pmid: 18367085
25. E. O. Williams *et al*., Delta Protocadherin 10 is Regulated by Activity in the Mouse Main Olfactory System. *Front. Neural Circuits* **5**, 9 (2011). doi: 10.3389/fncir.2011.00009; pmid: 21897809
26. G. Mountoufaris *et al*., Multicluster Pcdh diversity is required for mouse olfactory neural circuit assembly. *Science* **356**, 411–414 (2017). doi: 10.1126/science.aai8801; pmid: 28450637
27. N. Ihara, A. Nakashima, N. Hoshina, Y. Ikegaya, H. Takeuchi, Differential expression of axon-sorting molecules in mouse olfactory sensory neurons. *Eur. J. Neurosci.* **44**, 1998–2003 (2016). pmid: 27207328
28. J. Reisert, Origin of basal activity in mammalian olfactory receptor neurons. *J. Gen. Physiol.* **136**, 529–540 (2010). doi: 10.1085/jgp.201010528; pmid: 20974772
29. T. Connelly, A. Savigner, M. Ma, Spontaneous and sensory-evoked activity in mouse olfactory sensory neurons with defined odorant receptors. *J. Neurophysiol.* **110**, 55–62 (2013). doi: 10.1152/jn.00910.2012; pmid: 23596334

30. E. A. Hallem, M. G. Ho, J. R. Carlson, The molecular basis of odor coding in the Drosophila antenna. *Cell* **117**, 965–979 (2004). doi: 10.1016/j.cell.2004.05.012; pmid: 15210116
31. A. Dahanukar, E. A. Hallem, J. R. Carlson, Insect chemoreception. *Curr. Opin. Neurobiol.* **15**, 423–430 (2005). doi: 10.1016/j.conb.2005.06.001; pmid: 16006118
32. C. Y. Su, K. Menuz, J. R. Carlson, Olfactory perception: Receptors, cells, and circuits. *Cell* **139**, 45–59 (2009). doi: 10.1016/j.cell.2009.09.015; pmid: 19804753
33. R. J. Pasterkamp, J. J. Peschon, M. K. Spriggs, A. L. Kolodkin, Semaphorin 7A promotes axon outgrowth through integrins and MAPKs. *Nature* **424**, 398–405 (2003). doi: 10.1038/nature01790; pmid: 12879062
34. L. J. Brunet, G. H. Gold, J. Ngai, General anosmia caused by a targeted disruption of the mouse olfactory cyclic nucleotide-gated cation channel. *Neuron* **17**, 681–693 (1996). doi: 10.1016/S0896-6273(00)80200-7; pmid: 8893025
35. T. W. Chen *et al*., Ultrasensitive fluorescent proteins for imaging neuronal activity. *Nature* **499**, 295–300 (2013). doi: 10.1038/nature12354; pmid: 23868258
36. C. L. Torborg, M. B. Feller, Spontaneous patterned retinal activity and the refinement of retinal projections. *Prog. Neurobiol.* **76**, 213–235 (2005). doi: 10.1016/j.pneurobio.2005.09.002; pmid: 16280194
37. M. Meister, R. O. Wong, D. A. Baylor, C. J. Shatz, Synchronous bursts of action potentials in ganglion cells of the developing mammalian retina. *Science* **252**, 939–943 (1991). doi: 10.1126/science.2035024; pmid: 2035024
38. T. McLaughlin, C. L. Torborg, M. B. Feller, D. D. O'Leary, Retinotopic map refinement requires spontaneous retinal waves during a brief critical period of development. *Neuron* **40**, 1147–1160 (2003). doi: 10.1016/S0896-6273(03)00790-6; pmid: 14687549
39. T. A. Seabrook, T. J. Burbridge, M. C. Crair, A. D. Huberman, Architecture, Function, and Assembly of the Mouse Visual System. *Annu. Rev. Neurosci.* **40**, 499–538 (2017). doi: 10.1146/annurev-neuro-071714-033842; pmid: 28772103
40. A. Fleischmann *et al*., Mice with a "monoclonal nose": Perturbations in an olfactory map impair odor discrimination. *Neuron* **60**, 1068–1081 (2008). doi: 10.1016/j.neuron.2008.10.046; pmid: 19109912
41. M. Q. Nguyen, Z. Zhou, C. A. Marks, N. J. Ryba, L. Belluscio, Prominent roles for odorant receptor coding sequences in allelic exclusion. *Cell* **131**, 1009–1017 (2007). doi: 10.1016/j.cell.2007.10.050; pmid: 18045541
42. A. Vassalli, A. Rothman, P. Feinstein, M. Zapotocky, P. Mombaerts, Minigenes impart odorant receptor-specific axon guidance in the olfactory bulb. *Neuron* **35**, 681–696 (2002). doi: 10.1016/S0896-6273(02)00793-6; pmid: 12194868
43. L. Madisen *et al*., A toolbox of Cre-dependent optogenetic transgenic mice for light-induced activation and silencing. *Nat. Neurosci.* **15**, 793–802 (2012). doi: 10.1038/nn.3078; pmid: 22446880
44. R. O. Wong, M. Meister, C. J. Shatz, Transient period of correlated bursting activity during development of the mammalian retina. *Neuron* **11**, 923–938 (1993). doi: 10.1016/0896-6273(93)90122-8; pmid: 8240814
45. M. B. Feller, D. P. Wellis, D. Stellwagen, F. S. Werblin, C. J. Shatz, Requirement for cholinergic synaptic transmission in the propagation of spontaneous retinal waves. *Science* **272**, 1182–1187 (1996). doi: 10.1126/science.272.5265.1182; pmid: 8638165
46. B. K. Kobilka, X. Deupi, Conformational complexity of G-protein-coupled receptors. *Trends Pharmacol. Sci.* **28**, 397–406 (2007). doi: 10.1016/j.tips.2007.06.003; pmid: 17629961
47. R. A. Bond, A. P. Ijzerman, Recent developments in constitutive receptor activity and inverse agonism, and their potential for GPCR drug discovery. *Trends Pharmacol. Sci.* **27**, 92–96 (2006). doi: 10.1016/j.tips.2005.12.007; pmid: 16406086
48. M. Pyrski *et al*., Trpm5 expression in the olfactory epithelium. *Mol. Cell. Neurosci.* **80**, 75–88 (2017). doi: 10.1016/j.mcn.2017.02.002; pmid: 28188885
49. M. Pyrski *et al*., P/Q Type Calcium Channel Cav2.1 Defines a Unique Subset of Glomeruli in the Mouse Olfactory Bulb. *Front. Cell. Neurosci.* **12**, 295 (2018). doi: 10.3389/fncel.2018.00295; pmid: 30233329
50. N. Kanageswaran *et al*., Deep sequencing of the murine olfactory receptor neuron transcriptome. *PLOS ONE* **10**, e0113170 (2015). doi: 10.1371/journal.pone.0113170; pmid: 25590618
51. M. Omura, P. Mombaerts, Trpc2-expressing sensory neurons in the main olfactory epithelium of the mouse. *Cell Rep.* **8**, 583–595 (2014). doi: 10.1016/j.celrep.2014.06.010; pmid: 25001287
52. M. Behar, A. Hoffmann, Understanding the temporal codes of intra-cellular signals. *Curr. Opin. Genet. Dev.* **20**, 684–693 (2010). doi: 10.1016/j.gde.2010.09.007; pmid: 20956081
53. K. M. Tyssowski *et al*., Different Neuronal Activity Patterns Induce Different Gene Expression Programs. *Neuron* **98**, 530–546.e11 (2018). doi: 10.1016/j.neuron.2018.04.001; pmid: 29681534
54. E. Smedler, P. Uhlén, Frequency decoding of calcium oscillations. *Biochim. Biophys. Acta* **1840**, 964–969 (2014). doi: 10.1016/j.bbagen.2013.11.015; pmid: 24269537
55. H. Fujii *et al*., Nonlinear decoding and asymmetric representation of neuronal input information by CaMKIIα and calcineurin. *Cell Rep.* **3**, 978–987 (2013). doi: 10.1016/j.celrep.2013.03.033; pmid: 23602566
56. N. C. Spitzer, Electrical activity in early neuronal development. *Nature* **444**, 707–712 (2006). doi: 10.1038/nature05300; pmid: 17151658
57. P. L. Greer, M. E. Greenberg, From synapse to nucleus: Calcium-dependent gene transcription in the control of synapse development and function. *Neuron* **59**, 846–860 (2008). doi: 10.1016/j.neuron.2008.09.002; pmid: 18817726
58. Y. Chen, A. Ghosh, Regulation of dendritic development by neuronal activity. *J. Neurobiol.* **64**, 4–10 (2005). doi: 10.1002/neu.20150; pmid: 15884010
59. A. E. West, M. E. Greenberg, Neuronal activity-regulated gene transcription in synapse development and cognitive function. *Cold Spring Harb. Perspect. Biol.* **3**, a005744 (2011). doi: 10.1101/cshperspect.a005744; pmid: 21555405
60. S. W. Flavell, M. E. Greenberg, Signaling mechanisms linking neuronal activity to gene expression and plasticity of the nervous system. *Annu. Rev. Neurosci.* **31**, 563–590 (2008). doi: 10.1146/annurev.neuro.31.060407.125631; pmid: 18558867
61. T. P. Patel, K. Man, B. L. Firestein, D. F. Meaney, Automated quantification of neuronal networks and single-cell calcium dynamics using calcium imaging. *J. Neurosci. Methods* **243**, 26–38 (2015). doi: 10.1016/j.jneumeth.2015.01.020; pmid: 25629800
62. C. J. van Rijsbergen, *Information Retrieval* (Butterworths, ed. 2, 1979).

ACKNOWLEDGMENTS

We thank Y. Yoshihara for providing the *pGoofy-Cre* mice, H. Sakano for providing the *Kirrel2* conditional KO mice, and C. Greer, S. L. Zipursky, and K. Katori for their valuable comments. **Funding:** Supported by the Mitsubishi Foundation, the Takeda Science Foundation, the Japan Foundation for Applied Enzymology, the Kato Memorial Bioscience Foundation, the Japan Science and Technology Agency, PRESTO, JST ERATO grant JPMJER1801, the Human Frontier Science Program (RGP0019/2016), JSPS Grants-in-Aid for Scientific Research grant 18H05525, and JSPS KAKENHI grants 24370087, 15K21029, and 18K14712. This work was conducted partially as a program at the International Research Center for Neurointelligence (WPI-IRCN) of the University of Tokyo Institutes for Advanced Study. **Author contributions:** A.N., N.I., Y.I., and H.T. conceived the experiments; A.N., N.I., M.S., H.K., and H.T. performed the experiments and analyzed the data; all authors contributed to the writing the manuscript and provided helpful comments; and all authors read and approved the final manuscript. **Competing interests:** Authors declare no competing interests. **Data and materials availability:** All data are available in the manuscript or supplementary materials. All materials can be requested from H.T.

SUPPLEMENTARY MATERIALS

science.sciencemag.org/content/365/6448/eaaw5030/suppl/DC1
Figs. S1 to S12
Movies S1 and S2
Data S1 to S7

3 January 2019; accepted 23 May 2019
Published online 6 June 2019
10.1126/science.aaw5030

Structured spike series specify gene expression patterns for olfactory circuit formation

Ai Nakashima, Naoki Ihara, Mayo Shigeta, Hiroshi Kiyonari, Yuji Ikegaya and Haruki Takeuchi

Science **365** (6448), eaaw5030.
DOI: 10.1126/science.aaw5030originally published online June 6, 2019

Temporal code underlies circuit formation

Olfactory neurons respond to various odorants according to which olfactory receptors, of many, they express. During development, axons from olfactory neurons that express the same olfactory receptor converge to share the same glomeruli. Nakashima *et al.* now show that, in mice, the neurons build these connections according to shared patterns of activity. When the olfactory receptor is triggered, it causes its cell not simply to fire but to fire in specific patterns. Neurons that speak the same code end up connected at the same glomerulus.

Science, this issue p. eaaw5030